

Contribution of Tropical Waves to the Formation of Supertyphoon Megi (2010)

JUAN FANG

Key Laboratory of Mesoscale Severe Weather (MOE), School of Atmospheric Sciences, Nanjing University, Nanjing, China

FUQING ZHANG

Department of Meteorology, and Center for Advanced Data Assimilation and Predictability Techniques (ADAPT), The Pennsylvania State University, University Park, Pennsylvania

(Manuscript received 26 June 2015, in final form 28 March 2016)

ABSTRACT

Through observational analysis and numerical simulations, this study examines the roles of the Madden–Julian oscillation (MJO) and tropical waves in the three-stage formation of Supertyphoon Megi (2010) including 1) convective bursts followed by vorticity aggregation, 2) vortex rearrangement during decaying convection, and 3) convective reinvigoration and vortex intensification. The MJO was responsible for preconditioning the large-scale circulation and low-level moisture favorable for convection during all stages, while the counterpropagating Kelvin and equatorial Rossby (ER) waves brought low-level convergence and cyclonic vorticity anomalies to enhance massive convection in the western tropical Pacific in stage 1. Convection strengthened the vorticity anomalies nearby, which subsequently developed into Megi’s embryo by the end of stage 1 through merging with the positive vorticity anomaly carried by a westward-propagating mixed Rossby–gravity and tropical depression (MRG–TD)-type wave. The ER- and MRG–TD-type waves might also contribute to Megi’s formation through increasing low-level southwesterlies to the southwest of the precursor during stages 2 and 3. These tropical waves also indirectly affect Megi’s genesis through modulating surroundings near the precursor. Without the MJO, the low-level vorticity anomaly to the near west of the precursor would intensify more effectively and develop into a tropical cyclone instead of the observed Megi. Removing the Kelvin or ER wave would enhance convection to the far west of Megi’s precursor, which was less favorable for low-level convergence in the region of the precursor, and thus the formation of Megi.

1. Introduction

Tropical cyclone (TC) formation involves interactions among physical processes that vary over multiple space and time scales. Besides the favorable large-scale, climatological conditions as summarized by [Gray \(1968\)](#), the convectively coupled tropical waves including the Madden–Julian oscillation (MJO) also play vital roles in the formation of individual TCs that occurs infrequently and sporadically in the large areas of favorable environment conditions.

As the primary controller of the intraseasonal variability in the tropical atmosphere, the MJO is found to

be important to tropical cyclogenesis in most of the tropical ocean basins ([Schreck et al. 2012](#)). [Liebmann et al. \(1994\)](#) argued that twice as many TCs developed in association with negative MJO-filtered OLR anomalies as with positive anomalies in the northwestern Pacific and Indian Oceans. [Maloney and Hartmann \(2000a\)](#) showed that hurricanes are over four times more numerous during the westerly phases of the MJO than during the easterly phases in the northeastern Pacific. [Bessafi and Wheeler \(2006\)](#) suggested that the MJO produced significant basinwide modulations of cyclogenesis in the southern Indian Ocean. The MJO can affect the TC genesis through enhancing large-scale low-level convergence and meridional cyclonic shear and causing easterly vertical wind shear anomalies during its enhanced convection phase ([Maloney and Hartmann 1998, 2000b](#); [Bessafi and Wheeler 2006](#); [Frank and Roundy 2006](#); [Molinari et al. 1997](#)).

Corresponding author address: Dr. Juan Fang, Key Laboratory of Mesoscale Severe Weather (MOE), School of Atmospheric Sciences, Nanjing University, 163 Xianlin Road, Nanjing 210023, China.
E-mail: fangjuan@nju.edu.cn

The convective envelope of MJO is often accompanied by convectively coupled equatorial Rossby (ER) waves (Zhang 2005; Matthews 2004; Janicot et al. 2009; Masunaga 2007). Schreck and Molinari (2009) and Schreck et al. (2012) found that the ER waves are the most important tropical disturbance to TCs, especially for the twin TC formation across the equator. Ching et al. (2010) argued that the ER wave contributed notably to the record-breaking tropical cyclogenesis event that happened in the northwestern Pacific during June 2004. Bessafi and Wheeler (2006) proposed that the ER wave could modulate the environmental flows of TC genesis via its perturbations to convection and vorticity while Molinari et al. (2007) proposed that the ER wave increases the likelihood of TC formation via providing convergence and easterly vertical wind shear to promote wave energy trapping and accumulation.

The role of Kelvin waves in tropical cyclogenesis is an issue without consensus in literature. Bessafi and Wheeler (2006) and Frank and Roundy (2006) indicated that Kelvin waves may not play a vital role in TC genesis while Ventrice et al. (2012a,b) and Schreck (2015) found that tropical cyclogenesis becomes most frequent after the passage of a convective phase of Kelvin waves. The case studies of Schreck and Molinari (2011) and Ventrice et al. (2012a) showed that Kelvin waves are deeply involved in the genesis of Typhoon Rammason (2002), Typhoon Chataan (2002), and Tropical Storm Debby (2006). It is found that the Kelvin wave can reduce (enhance) westerly (easterly) vertical wind shear and increase atmospheric moisture and low-level potential vorticity (Schreck and Molinari 2011; Ventrice et al. 2012a,b).

Different from the above-mentioned waves, the mixed Rossby–gravity (MRG) and tropical depression (TD)-type waves affect TC genesis mainly by providing seedlings of TCs. Dunkerton et al. (2009) pointed out that the critical layer of easterly waves, the spectrum of which covers the MRG- and TD-type waves, could be a “pouch” or “sweet spot” for TC formation. Schreck et al. (2012) also found that the TD-type waves were the primary initial disturbance of TCs over the Northern Hemisphere. Xu et al. (2013) suggested that the TD-type wave accounts for about 96% of TC genesis in the northwestern Pacific during the 2008/09 typhoon seasons where the TD-type waves usually provide seedlings of TCs. The MRG waves are important sources of off-equatorial TD-type waves (Takayabu and Nitta 1993; Liebmann and Hendon 1990). Dickinson and Molinari (2002) documented a case where the westward-moving MRG waves transformed to northwestward-moving TD-type waves and led to the genesis of three TCs in the northwestern Pacific. The idealized simulation

performed by Aiyyer and Molinari (2003) showed that amplification of the MRG waves led to a series of small-scale off-equatorial TD-type disturbances under an MJO-like basic state. Based on the statistical analysis and numerical simulations, Chen and Huang (2009) and Chen (2012) investigated favorable conditions for the transition from MRG waves to TD-type disturbances and found that ENSO could modulate the transition over the northwestern Pacific.

TC genesis can often be associated with several types of tropical waves. Hogsett and Zhang (2010) suggested that the MJO, Kelvin, and MRG waves likely all have contributed to the formation of Typhoon Chanchu (2006). Shen et al. (2012) and Shu and Zhang (2015) presented the formation of TCs in association with an MRG wave during an active phase of the MJO. Chen and Chou (2014) noticed that the TC genesis related to multiple waves was roughly twice as many as those related to a single wave. They suggested that the joint contribution from more than one wave type favors creating a coherent environment favorable for TC formation.

This study examines the formation of Supertyphoon Megi (2010) from several initially sporadic vorticity anomalies in the western tropical Pacific Ocean with a focus on the joint effects of tropical waves through observational analysis and convection-permitting sensitivity experiments. The data and methodology are described in section 2. Section 3 presents the synoptic background behind this case. In section 4, the roles of the MJO and tropical waves in the formation of Megi are discussed. Concluding remarks are given in section 5.

2. Data and methods

The 6-hourly Global Forecast System (GFS) analysis fields at 0.5° resolution from the U.S. National Centers for Environmental Prediction (NCEP) were used for observational analysis. The information about Megi was obtained from the best-track data of the Japan Meteorological Agency (JMA). The convective activity in the genesis of Megi was analyzed with the blackbody temperature (TBB) derived from the Japanese Geostationary Meteorological Satellite (GMS)/Multifunctional Transport Satellite (MTSAT) and the Tropical Rainfall Measuring Mission (TRMM) Multisatellite Precipitation Analysis (product 3B42; Huffman et al. 2007).

To diagnose the MJO and tropical waves, the filters originally proposed by Wheeler and Kiladis (1999) were applied to the TRMM rainfall data. Prior to filtering, TC-related rainfall has been removed following Schreck et al. (2011). The filter bands of periods and wave-numbers adopted here are similar to those in Schreck

et al. (2012)—that is, MJO: 30–96 and 0–9 days, Kelvin wave: 2.5–17 and 1–14 days, ER wave: 9–72 and from –10 to –1 days, MRG wave: 3–10 and from –10 to –1 days, and TD-type wave: 2.5–5 and from –20 to –6 days.

The fully compressible Weather Research and Forecasting (WRF) Model (version 3.5.1; Skamarock and Klemp 2008) was used for the evaluation of the roles of the MJO and tropical waves in the formation of Megi via performing control and sensitivity experiments. The model domain was triply nested through two-way nesting with horizontal grid spacings of 13.5, 4.5, and 1.5 km and mesh sizes of 481×361 , 811×601 , and 811×691 grid points, respectively. The model has 35 levels with the model top at 10 hPa. The physics packages used here include the WRF single-moment (WSM) 6-class microphysics scheme (with graupel) (Hong et al. 2004), Yonsei University (YSU) boundary layer scheme (Noh et al. 2003), the Rapid Radiative Transfer Model (RRTM) for longwave radiation (Mlawer et al. 1997), and the Dudhia shortwave radiation scheme (Dudhia 1989). To better simulate the large-scale circulation of Megi formation, spectrum nudging was applied to the outermost domain to nudge the disturbances with the scale larger than 810 km to the GFS analysis data during the 5-day simulation. In the inner domains, the spectrum nudging was also used in the first 24-h integration with the aim to reduce the impact of cold start of the simulation. The model was initialized with the 0.5° GFS analysis at 0600 UTC 8 October.

3. Synoptic background

Megi was the strongest TC over the globe in 2010 whose sudden track changes as well as unusual intensity and cold wake drew the attention of several studies (e.g., Kieu et al. 2012; Qian et al. 2013; Shi et al. 2014; Wang and Wang 2013, 2014; Ko et al. 2014). The current study focuses on its formation under the influences of the MJO and tropical waves that were not fully explored in literature.

a. A three-stage genesis of Megi

The origin of Megi was closely linked with several tropical disturbances with positive vorticity anomalies (PVAs) initially scattered in the western tropical Pacific Ocean. Figure 1 sketches the evolution of the PVAs for the week leading up to Megi genesis. From Fig. 1a we can see the PVAs located between 4° and 12°N over the western tropical Pacific at 0000 UTC 6 October, with the easternmost two PVAs (“A” and “C”) at around 180° and 160°E , respectively. It is apparent that PVA A was related to an easterly wave. As the PVAs moved westward (Figs. 1b–e), strengthened by two episodes of massive deep convection, PVA C intensified and

broadened while a new PVA (“B”) began to emerge at its northeast side. In the meanwhile, the 850-hPa winds shifted from east-southeast to south-southwest at the southeast side of PVA C. This shift led to increased low-level convergence and positive vorticity to the northeast of PVA C and slowdown in the westward movement of PVA B (Figs. 1c–e). At 0600 UTC 9 October (Fig. 1e), the further intensified PVA B was caught up by PVA A to form a larger PVA (“M”), which was the embryo of Megi.

From 0600 UTC 9 October (Figs. 1e,f), deep convection began to decay in the western tropical Pacific. The area with $\text{TBB} < -40^\circ\text{C}$ shrunk gradually with little around PVA M. As the convection weakened, the low-level southwesterly flow drove the enhanced positive vorticity in the northeastern tip of PVA C northeastward (Fig. 1e), so that PVA M incorporated the positive vorticity to evolve into a larger and more organized PVA at 0600 UTC 10 October (Figs. 1e,f). After that, deep convection reburst and strengthened from sporadic to well organized in the area of PVA M (Figs. 1f–i). At the same time, the low-level southwesterly flow was enhanced at the southeast side of PVA C. Under the help of the southwesterly flow, the vorticity at the northeastern tip of PVA C was captured by the westward-moving PVA M as that occurred in the period from 0600 UTC 9 October to 0600 UTC 10 October. Consequently, PVA M intensified rapidly and became a tropical depression (TD) at around 0000 UTC 13 October (Fig. 1j).

From the variations of convection and PVAs described above, the formation of Megi can be roughly categorized into three stages (with 0600 UTC 9 October and 0600 UTC 10 October subjectively chosen as the dividing points): 1) massive convective burst, vorticity aggregation, and formation of Megi embryo; 2) decaying convection and vortex rearrangement; and 3) deep convection reinvigoration, vortex intensification, and formation of Megi.

b. Activity of the tropical waves in the formation of Megi

Similar to the formation of most TCs, the genesis of Megi was deeply influenced by tropical waves including the MJO. Figure 2 shows the time–longitude section of unfiltered and MJO-filtered TRMM rainfall averaged between 5° and 15°N . It is clear that the genesis of Megi, which featured a two-episode massive convection (denoted by the thin ellipses) and then a westward-moving convective system, mainly occurred on the leading edge of an envelope of eastward-moving convection representative of the MJO. Even though the main body of MJO’s convective envelope and the related low-level

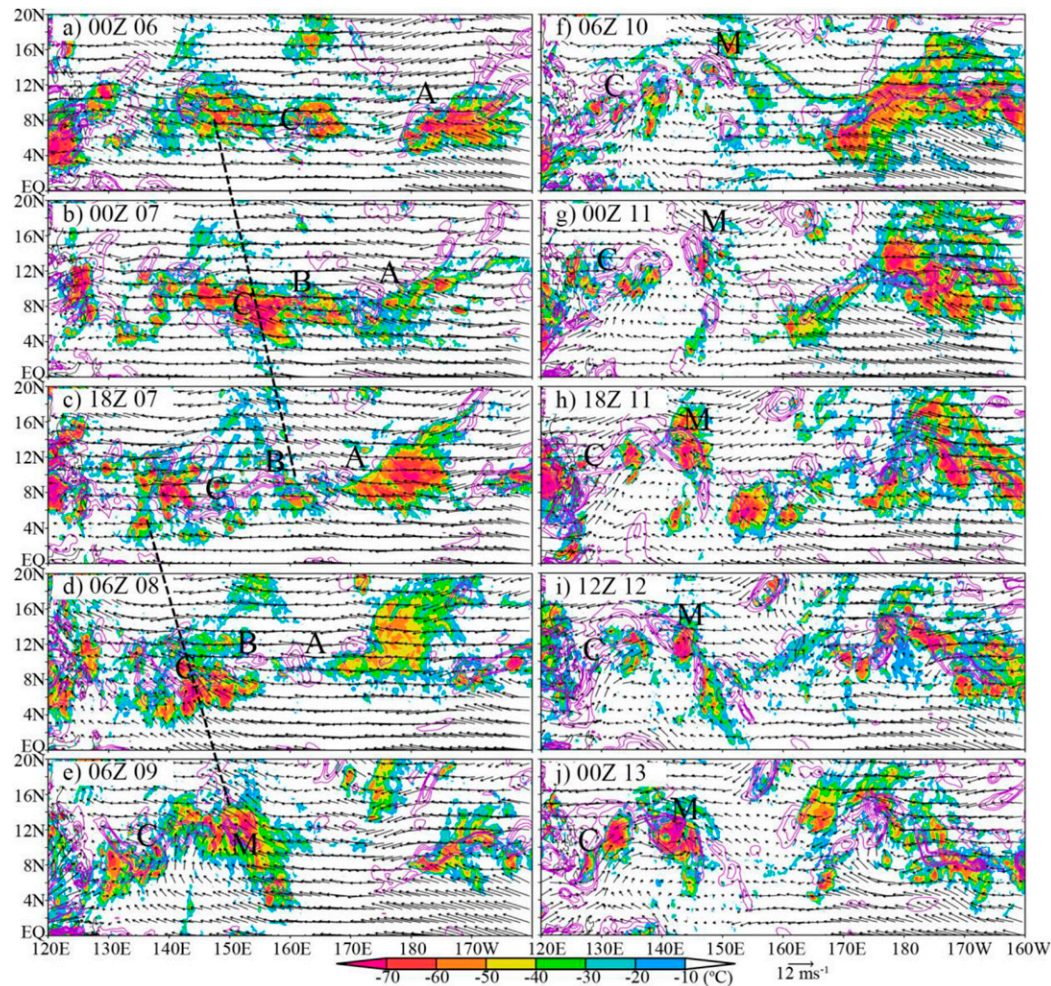


FIG. 1. The 850-hPa wind (vectors) and vorticity (contours) obtained from the GFS analysis as well as the blackbody temperature (shading) derived from GMS/MTSAT over the northern tropical Pacific from 0000 UTC 6 Oct to 0000 UTC 13 Oct 2010. The values of contours are 1×10^{-5} , 2×10^{-5} , 3×10^{-5} , 5×10^{-5} , 7×10^{-5} , 10×10^{-5} , 13×10^{-5} , 16×10^{-5} , 20×10^{-5} , 24×10^{-5} , and $28 \times 10^{-5} \text{ s}^{-1}$. The dashed lines and capital letters denote the two episodes of massive deep convection and positive vorticity anomalies, respectively.

westerly flow were to the far west of Megi's precursor, the MJO did precondition the large-scale environment in the northwestern Pacific by enhancing low-level convergence and cyclonic vorticity as well as low-to-midlevel relative humidity (Fig. 3a), which was favorable for the formation of Megi.

Figures 4 and 5 present maps of unfiltered and wave-filtered TRMM rainfall as well as 850-hPa relative vorticity for the week leading up to genesis. Consistent with that in Fig. 2, the MJO's convective envelope has penetrated to 170°E by 0000 UTC 6 October though its main body was still to the west of 130°E (Fig. 4a). In the convective envelope of the MJO, there are two successive Kelvin waves with the convective envelopes situated in the regions around 165° and 125°E , respectively. Though the off-equatorial pattern of Kelvin-wave-filtered

rainfall differs somewhat from the classical model described in Fig. 3f of Kiladis et al. (2009) (Fig. 4a), the horizontal structures of filtered fields—that is, the in-phase relationship between wind and height, the latitudinal symmetry of wind and height fields about the equator, and the zonal wind dominating the equatorial area—are all as predicted by theory (figures not shown). Furthermore, the estimated eastward phase speed of the Kelvin wave is about 12.9 m s^{-1} in this study, which is also in the range of the typical phase speeds of Kelvin waves (Wheeler and Kiladis 1999; Roundy 2008). The off-equatorial pattern of Kelvin-wave-filtered rainfall shown in Fig. 4a could be related to the asymmetry of moisture supply and conditional unstable energy due to complex oceanic and atmospheric environmental conditions in the northwestern Pacific Ocean.

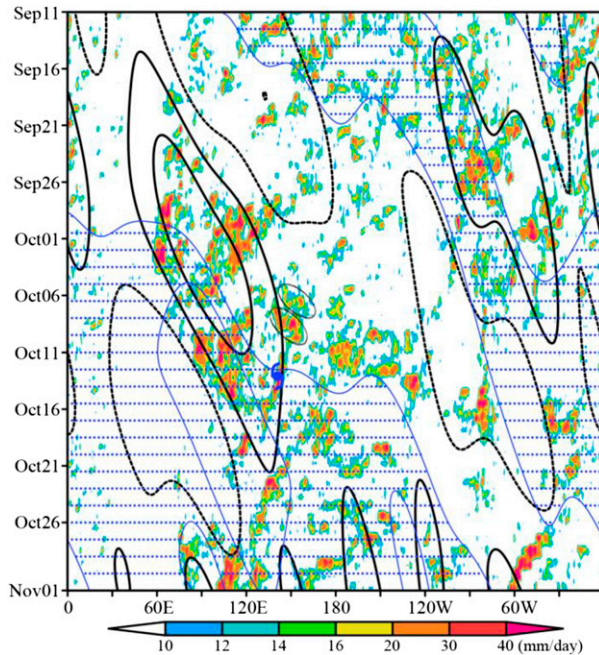


FIG. 2. Time-longitude section of unfiltered (shading) and MJO-filtered TRMM rainfall (black contours indicating -1.2 , 1.2 , and 3.6 mm day^{-1} with negative dashed) and 850-hPa zonal wind speed (blue contours indicating 0 and 2 m s^{-1}) averaged between 5° and 15°N . The tropical cyclone symbol marks the genesis time and location of Megi while the ellipses denote the two-episode massive deep convection related to Megi genesis. The region with westerly flow is stippled.

Counterpropagation to the MJO and Kelvin waves, PVAs C and A entered the convective envelopes of the MJO and Kelvin waves one after another experiencing two episodes of massive convection in the following several days (Figs. 4b–e). The overlapping between the massive deep convection and the convective envelopes of Kelvin waves indicates that the deep convection could be enhanced by the Kelvin waves in the MJO’s convective envelope. From Fig. 6a we can see that, as the moist phase of Kelvin waves propagated eastward, the accompanied low-level westerly anomaly approached the PVAs gradually from the west and led to noticeable convergence in the region embedding the PVAs after around 0000 UTC 8 October, which together with the positive low-level cyclonic vorticity and low-to-midlevel relative humidity anomalies induced by Kelvin waves was conducive to convection and vorticity enhancement in the PVAs and nearby (Fig. 3b). Moreover, PVA B and the northeastern tip of PVA C began to be covered by the convective envelope of an ER wave at around 0600 UTC 8 October (Figs. 4d,e). The ER wave also contributed to the increase of low-level convergence and vorticity in the region of the PVAs after about 1500 UTC 8 October (Fig. 3c). The counter propagating

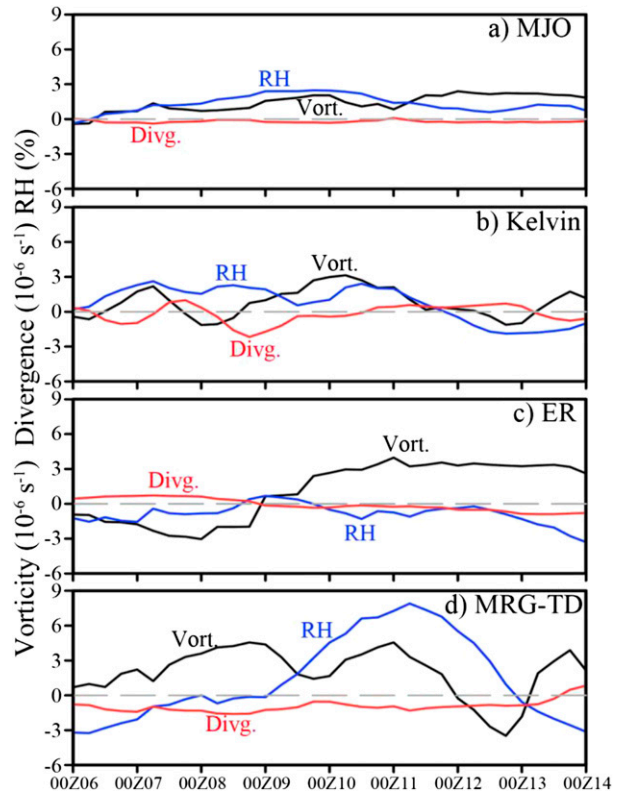


FIG. 3. Time evolution of area-mean (a) MJO-, (b) Kelvin-, (c) ER-, and (d) MRG-TD-filtered 850-hPa vorticity (black) and divergence (red) as well as 1000–500-hPa-averaged relative humidity (blue) in the domain centered at the center of Megi’s precursor with the radius of about 2° .

ER and Kelvin waves induced evident low-level westerly anomalies to the west of PVA B as well, which slowed down the westward movement of PVA B and prompted it to merge with PVA A (Figs. 6a,b).

In the favorable environment modified by the MJO, Kelvin, and ER waves, PVA C was notably strengthened and enlarged while PVA A merged with B to become the embryo of Megi (i.e., PVA M) at 0600 UTC 9 October (Fig. 4e). After that, the moist phase of Kelvin waves moved out of the region with PVA M gradually (Figs. 4e–j) while the ER wave continued to favor the development of PVA M via increasing the low-level convergence and cyclonic vorticity in the area around the PVA (Fig. 3c). Meanwhile, in agreement with the conceptual model depicted by Kiladis et al. (2009), the ER wave facilitated the development of low-level southwesterly flow to the southwest of PVA M (Figs. 6b,c). The intensified southwesterly flow not only increased the low-level convergence in the region of PVA M but also could promote PVA M to absorb the vorticity in the northeastern tip of PVA C over the period from 0600 UTC 9 October to 1800 UTC

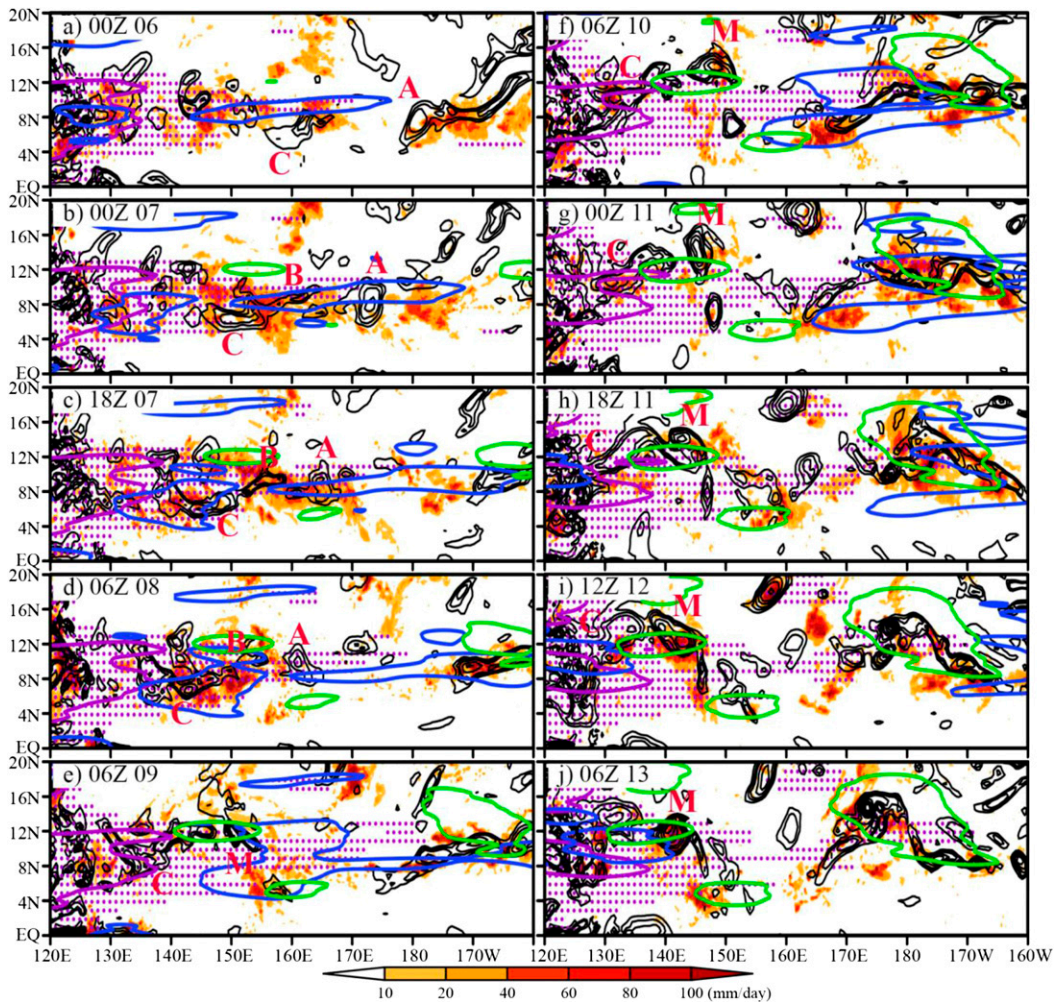


FIG. 4. The 850-hPa vorticity (black contours with values as in Fig. 1) and wind vectors obtained from the GFS analysis as well as unfiltered (shading), MJO- (purple contours), Kelvin- (blue contours), and ER-filtered (green contours) rainfall over the tropical Pacific for the week leading up to Megi's genesis. The contour values for the MJO- and wave-filtered rainfall are 3 and 4 mm day⁻¹, respectively. The areas with positive MJO-filtered rainfall are stippled.

11 October (Figs. 1e–h). Accompanied by the ER wave, PVA M developed into TD Megi at 0000 UTC 13 October.

During the formation of Megi, the convective envelopes of MRG- and TD-type waves appeared in the region around the PVAs from time to time (Fig. 5), which might have also contributed to the formation of Megi. From Figs. 5a–c, we can see that PVA A was initially carried by westward-moving MRG- and TD-type waves. Moreover, a convective envelope of a TD-type wave appeared at the southwest side of PVA M after about 0600 UTC 9 October. Since convection mainly occurred in the center area of low-level cyclonic circulation in a TD-type wave, the TD-type wave could also benefit the development of low-level southwesterly flow to the southwest of PVA M. Considering that the

MRG- and TD-type waves usually occupy an overlapping wavenumber–frequency space that is hard to separate in practice (Kiladis et al. 2009), we will refer to them together as an MRG–TD-type wave following previous studies in literature (e.g., Frank and Roundy 2006; Straub and Kiladis 2003; Ching et al. 2010). From Fig. 3d, we can see that the MRG–TD-type wave could favor the development of PVA M by inducing conspicuous low-level convergence, cyclonic vorticity, and moisture anomalies in the region of the PVA after around 0000 UTC 9 October. In addition, the MRG–TD-type wave might also contribute to the enhancement of low-level southwesterlies to the southwest of PVA M (Figs. 6d,e).

In brief summary, the three-stage formation of Megi closely related to the combined effect of tropical waves.

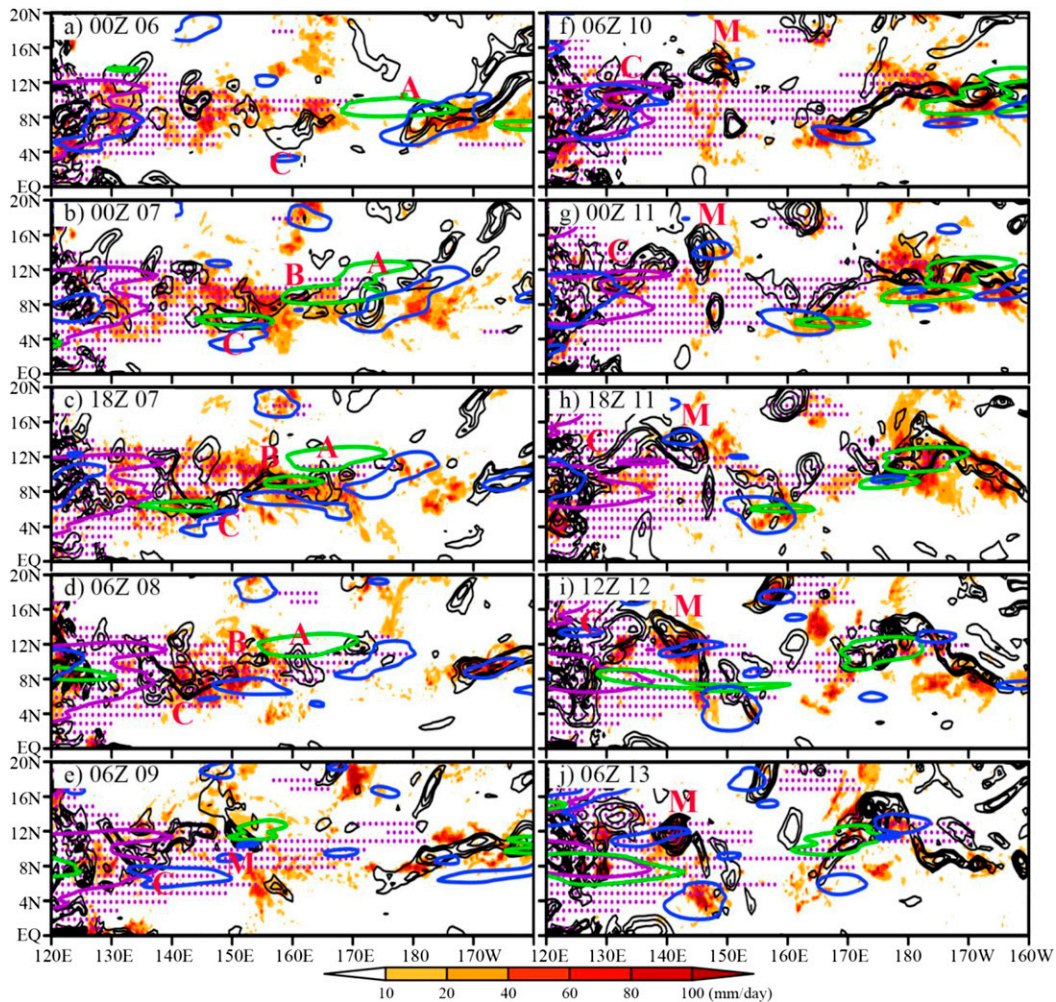


FIG. 5. As in Fig. 4, but for MRG- (green contours) and TD-filtered (blue contours) rainfall.

The MJO provided large-scale low-level convergence, cyclonic vorticity, and low-to-midlevel moisture favorable for convection and vorticity enhancement for all stages. In stage 1, the counterpropagating Kelvin and ER waves was conducive to massive deep convection and low-level westerly surges in the western tropical Pacific, which strengthened PVA B and promoted it to become Megi's embryo through merging with PVA A carried by the MRG-TD-type wave. In stages 2 and 3, the ER- and MRG-TD-type waves worked jointly to enhance low-level convergence and cyclonic vorticity in the region of PVA M and low-level southwesterlies to the southwest of the PVA and, thus, to facilitate Megi's embryo to develop into a TD.

4. Roles of the MJO and tropical waves in the formation of Megi

From Figs. 4 and 5, we can see that convection and vorticity in the western part of PVA C could be affected by the

MJO and tropical waves as well. Since TC genesis was deeply influenced by the surrounding environment, the tropical waves might also affect Megi's formation indirectly by modifying convection and vorticity in the western part of PVA C. In this section, the role of the MJO and each type of tropical wave, and the relative significance will be further examined through convection-permitting WRF simulations with the domain configuration shown in Fig. 7.

a. Tropical cyclogenesis in the control experiment

Figure 8a depicts the model-derived sea level pressure (SLP) and 10-m winds at 0000 UTC 13 October when JMA started to identify TD Megi centered at (11.9°N, 141.4°E) with the minimum SLP of 1006 hPa. From the figure, we can see that model-simulated TC situated at about (12.5°N, 142°E) with the minimum SLP of ~1006 hPa, which was very close to the best-track estimate of JMA. In addition, the tracks of Megi's precursor determined by the GFS- and model-derived 850-hPa

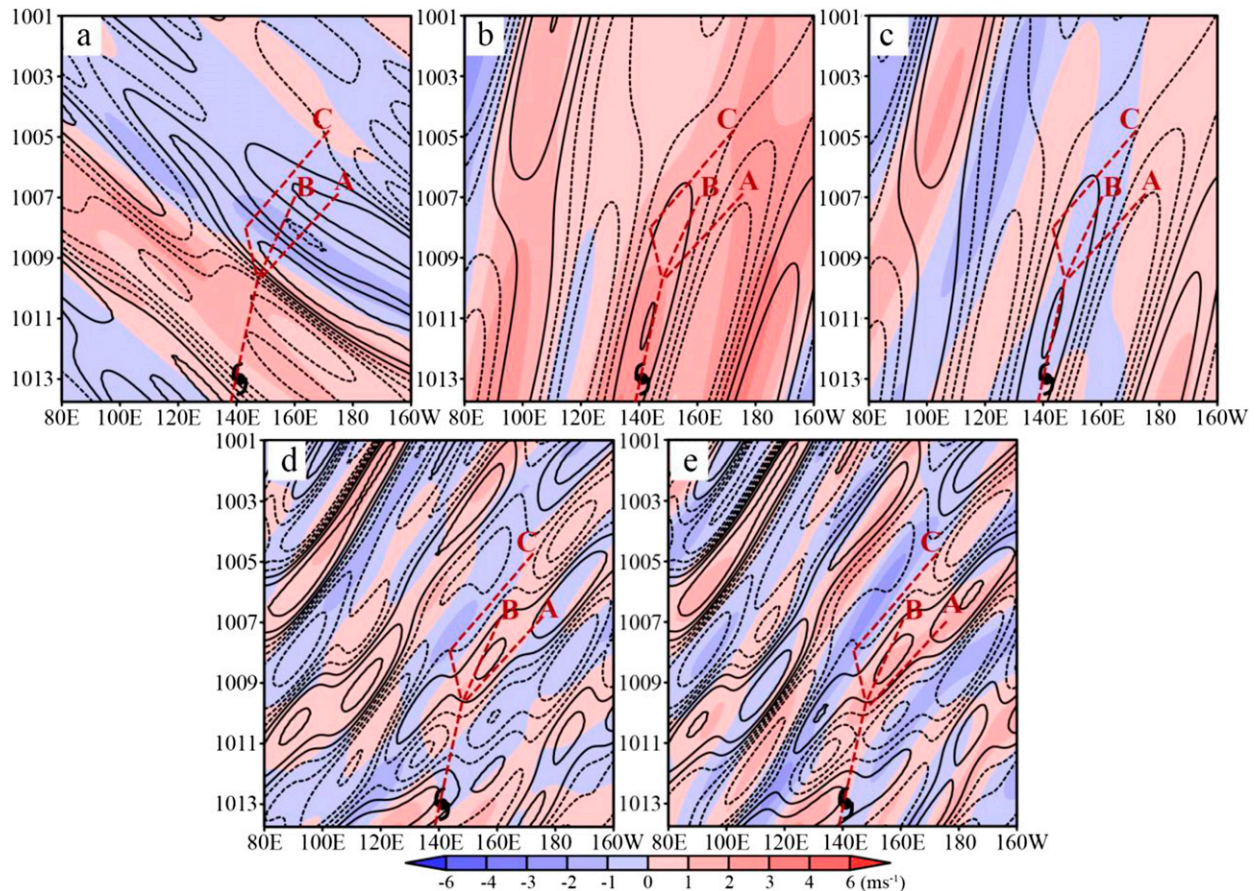


FIG. 6. (a) Time–longitude section of Kelvin-filtered 850-hPa zonal velocity (shading) and TRMM rainfall (contours) averaged between 5° and 15° N. (b) As in (a), but for the ER-filtered zonal velocity and rainfall. (c) As in (b), but for meridional velocity and rainfall. (d),(e) As in (b),(c), but for MRG–TD-filtered velocity and rainfall. The tropical cyclone symbols mark the genesis location of Megi. The letters A, B, and C and the pink dashed lines denote the vorticity anomalies related to Megi formation and their approximated tracks. The wave-filtered rainfall is contoured at -5 , -2.6 , -1.4 , -0.2 , 1.0 , 2.4 , and 4.8 mm day^{-1} with negative dashed.

vorticity shown in Fig. 8a indicate that the motion of the precursor was described by the model appropriately as well.¹

Figure 9 presents the evolution of model-simulated column-maximum reflectivity and 850-hPa winds and relative vorticity from 1200 UTC 8 October to 0000 UTC 12 October.² For convenience, the eastern and western parts of PVA C have been denoted as “C1” and “C2” in

¹ After the embryo (i.e., PVA M) develops, its location is defined as the vorticity centroid of a domain with a radius of 2° following Wang (2014). Before the embryo develops properly, the position of precursor is subjectively determined via tracing PVA B. To trace PVA B properly in the numerical simulations, the vorticity field was interpolated to the grids with 0.5° resolution first via Cressman interpolation.

² For convenience comparing the model- and GFS-derived results, the wind and vorticity derived from the model were interpolated to the grids with 0.5° resolution via Cressman interpolation.

Fig. 9, respectively. Consistent with observations, vigorous convection appeared in the western tropical Pacific after a 6-h spinup of the simulation (Figs. 9a–c). Correspondingly, the vorticity in the eastern end of PVA C, PVAs B and A, and nearby increased sequentially and aggregated simultaneously to form a large PVA (i.e., PVA M) at 0600 UTC 9 October (Fig. 9d). Along with the departure of Kelvin waves, the low-level convergence anomaly related to Kelvin wave weakened in the area of PVA M after about 0600 UTC 9 October (Fig. 3b). Meanwhile, owing to the sublimation and/or melting and evaporation of precipitation associated with the vigorous convection, a distinct low-level cold pool developed in the region around PVA M after 0600 UTC 9 October (figure not shown), which was unfavorable for the maintenance of severe convection in that region by inducing strong low-level divergence flow. As a result, convection decayed substantially in the region of PVA M and nearby after 0600 UTC 9 October (Figs. 9d,e). Similar to what

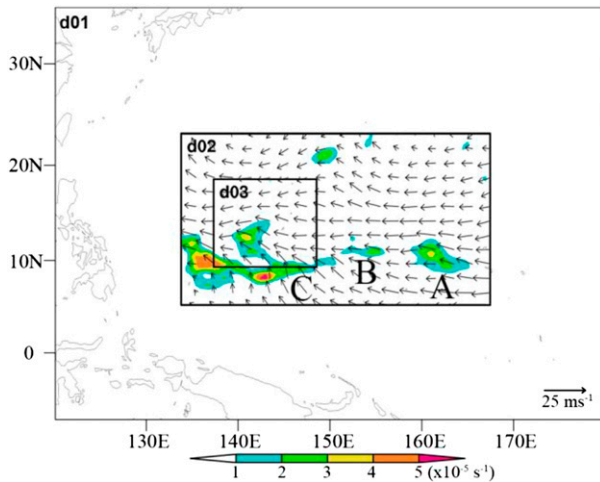


FIG. 7. Domain configuration for the numerical simulations. Vectors and shading in domain 2 depict the 850-hPa winds and vorticity obtained from the GFS analysis at 0600 UTC 8 Oct 2010.

occurred in observations, PVA M drew in the vorticity at the northeastern tip of PVA C (i.e., C1) under the help of low-level southwesterly flow that developed on its southwest side and gradually evolved into a larger PVA (i.e., PVA M) over the following 24 h (Figs. 9d,e). As the cold pool resulting from previous convection weakened

(likely as a result of the sensible heat flux from the warm ocean and the geostrophic adjustment of wind and pressure fields), convection became active again in the area of PVA M at around 0600 UTC 10 October (Figs. 9f-h). From Figs. 9e-g, we can see that the strengthened low-level southwesterlies to the southwest of PVA M enhanced convection and vorticity on its leading edge and then advected the vorticity to PVA M consistent with observations. Under the effect of convection and low-level southwesterly flow, PVA M spun up progressively to a TD at 0000 UTC 13 October.

From the above description, it can be concluded that the key processes occurring in the formation of Megi, such as initial deep convection, vorticity aggregation, low-level southwesterly surges, and convection reinvigoration, were well captured by the model. Hence, it was appropriate to take the model-derived tropical cyclogenesis as a benchmark to evaluate the influence of tropical waves on Megi's formation.

b. Tropical cyclogenesis in sensitivity experiments

Based on the control simulation (CNTRL) introduced in section 4a, five sensitivity experiments were performed with exactly the same configuration except that the initial and lateral boundary conditions as well as the fields used in the spectral nudging were modified by removing the

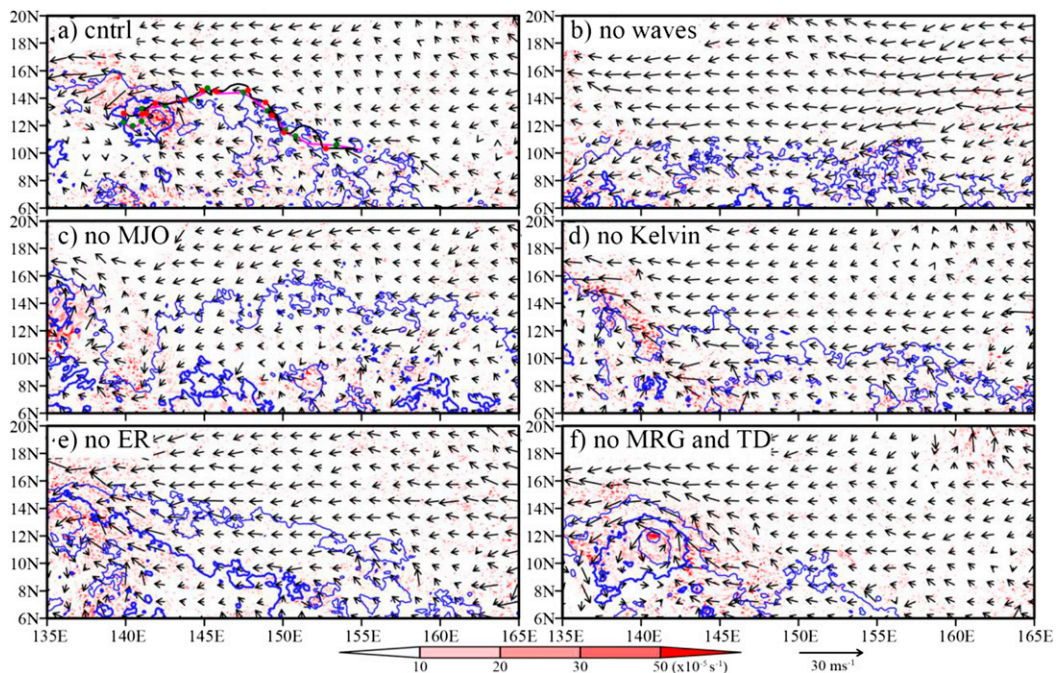


FIG. 8. The model-simulated 850-hPa wind (vectors), vorticity (shading), and sea level pressure (blue contours with an interval of 1 hPa) at 0000 UTC 13 Oct 2010. The maximum sea level pressure depicted by the contours is 1008 hPa. The black and pink lines depict the track of observed and CNTRL-derived Megi's precursor at 850 hPa, respectively. The position of Megi's precursor at 0000 and 1200 UTC is denoted with dots.

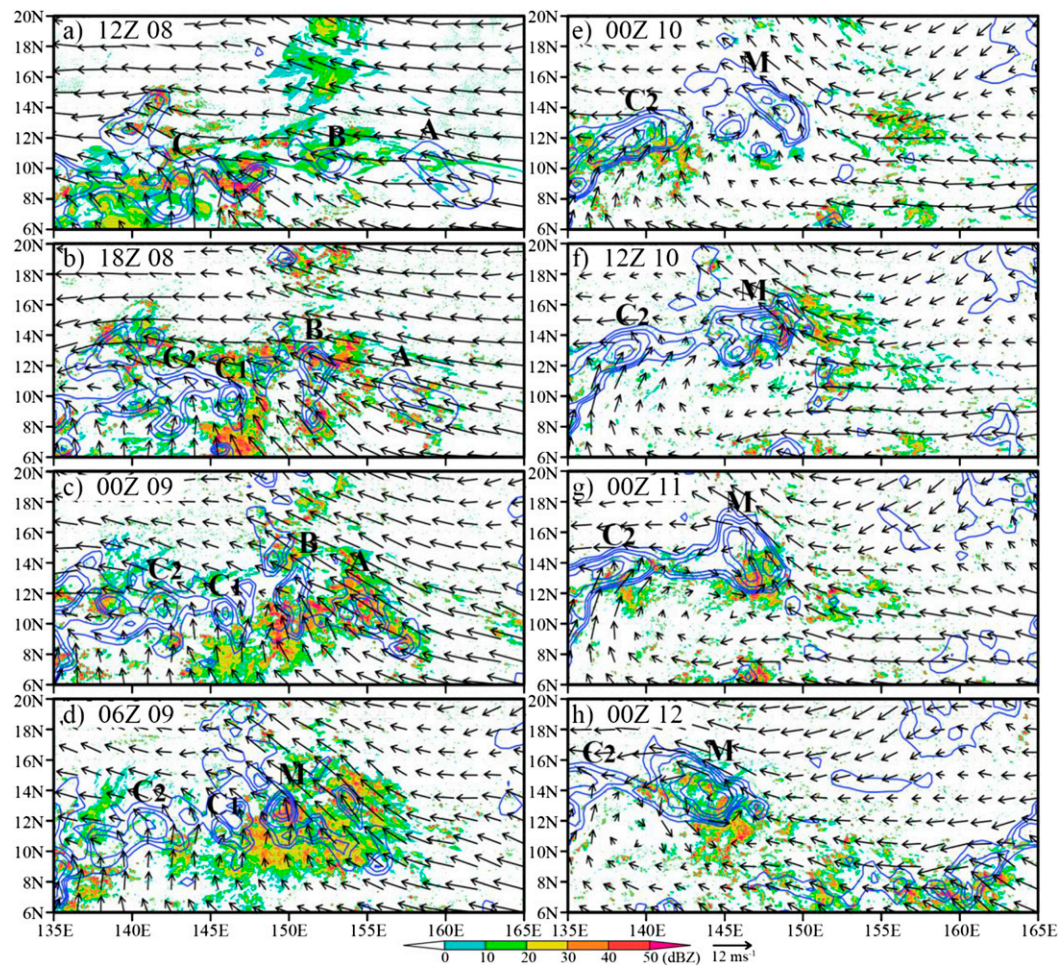


FIG. 9. The 850-hPa wind (vectors) and vorticity (contours with values as in Fig. 1) and the column-maximum reflectivity (shading) derived from the control simulation from 1200 UTC 8 Oct to 0000 UTC 12 Oct 2010. The capitals denote the positive vorticity anomalies.

signals of MJO (noMJO), Kelvin waves (noKelvin), ER waves (noER), MRG–TD-type waves (noMRG–TD), and all the above-mentioned waves including the MJO (noWaves), respectively. Figure 10 demonstrates the differences of initial fields in the sensitivity experiments from that in CNTRL in the lower troposphere. It is obvious that the removal of waves modified the dynamic and thermodynamic fields considerably in the northwestern Pacific and, thus, affected the evolution of the PVAs in that region and, likely later, the genesis of Megi.

From Figs. 8b–f we can see that, except for noMRG–TD, the other four sensitivity experiments failed to produce TCs at the location and time close to that derived from CNTRL. In noWaves (Fig. 8b), neither closed isobar of sea level pressure nor near-surface cyclonic circulation similar to that of a TC could be identified at 0000 UTC 13 October. Though a TC developed at 0000 UTC 13 October in noMJO (Fig. 8c), it was

located at around (14°N, 136°E), more than 500 km away from that in CNTRL (and in observations). In noKelvin (Fig. 8d), there is a near-surface cyclonic circulation centered at about (10.5°N, 139°E) at 0000 UTC 13 October. However, it was not accompanied by closed isobars. On the contrary, the closed isobars appeared near (13°N, 136.5°E) while the closed cyclonic circulation did not properly develop at 0000 UTC 13 October in noER (Fig. 8e). In the rest of this section, the evolution of convection and PVAs in the sensitivity experiments will be discussed in detail to understand how these tropical waves affect the formation of Megi.

1) EVOLUTION OF PVAS AND CONVECTION IN NOWAVES

Because of the distinct low-level divergence anomaly induced by removing the tropical waves (Fig. 10b), convection simulated in noWaves was much weaker in

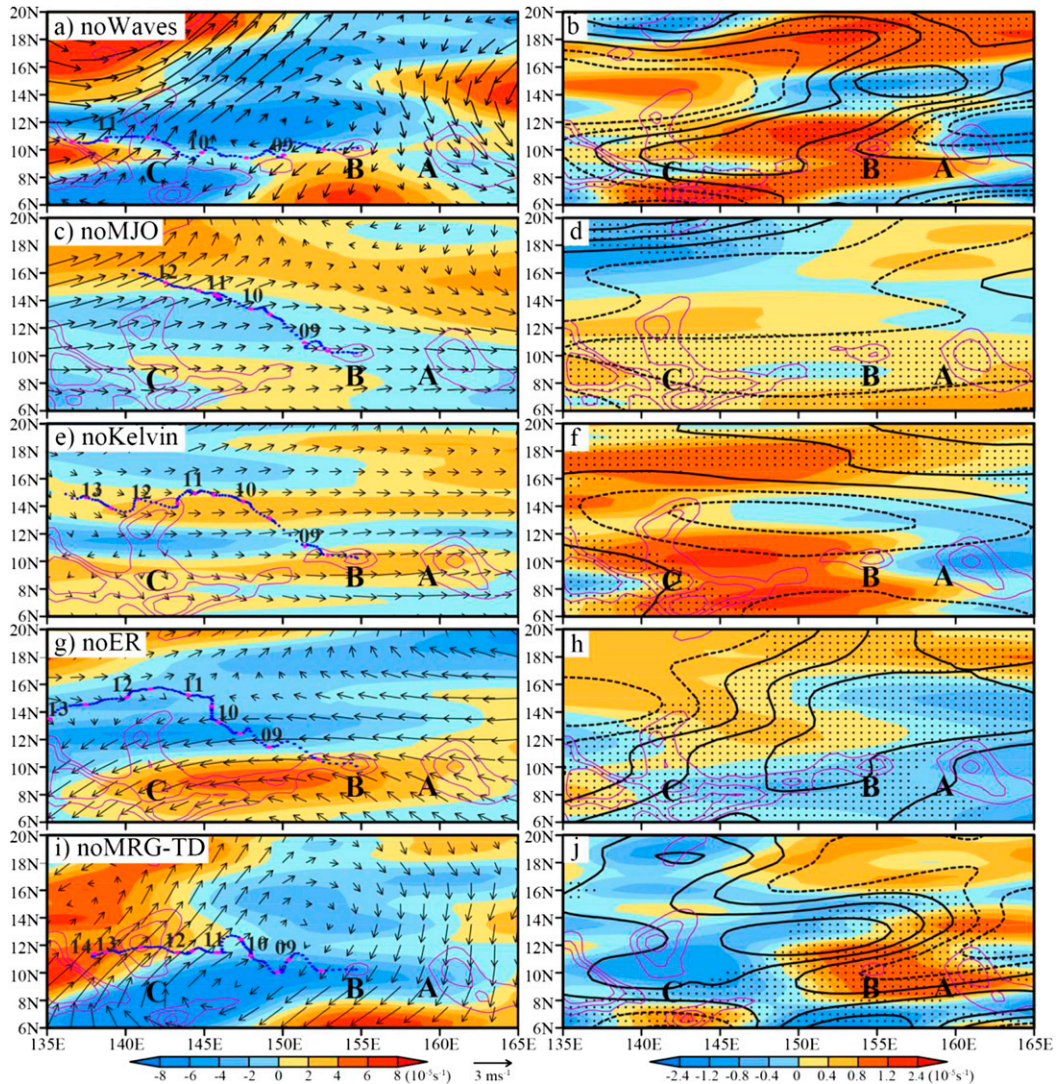


FIG. 10. (left) The differences of 850-hPa vorticity (shading) and winds (vectors) between the sensitivity and control experiments at 0600 UTC 8 Oct 2010. (right) As in (left), but for the 850-hPa divergence (shading) and 1000–700-hPa-averaged specific humidity (contours with values of 0, ± 0.2 , ± 0.4 , ± 0.8 , and $\pm 1.2 \text{ g Kg}^{-1}$). The purple thin contours depict the 850-hPa vorticity with values as in Fig. 1 and the capital letters denote the positive vorticity anomalies. The blue and pink dots designate the track of Megi’s precursor in (left). The numbers along the tracks denote the date. The area with positive surface-based CAPE anomalies is stippled in (right).

the northern tropical Pacific between 140° and 155°E than that in CNTRL (Fig. 11b). Consequently, the low-level easterly winds to the west of about 155°E did not weaken significantly and were much stronger than those in CNTRL after the start of simulation in noWaves (Fig. 12b). Because of the relatively stronger steering flow, the PVAs moved westward too fast to allow scale contraction and energy accumulation of the PVAs, both of which were found to be critical to TC development (Webster and Chang 1988; Holland 1995; Sobel and Maloney 2000; Maloney and Hartmann 2001). Hence, the intensification and aggregation of the PVAs as well

as the convection around them were comparatively weak before 0600 UTC 10 October in noWaves. Although PVA B intensified and slowed down as severe convection burst after around 0000 UTC 11 October (Fig. 12b), it failed to form a TC before it moved out of the middle domain of the model (Fig. 8b).

2) EVOLUTION OF PVAS AND CONVECTION IN NOMJO

Figures 11c and 12c manifest that the key processes that occurred in the formation of observed and CNTRL-simulated Megi—that is, initial vigorous convection,

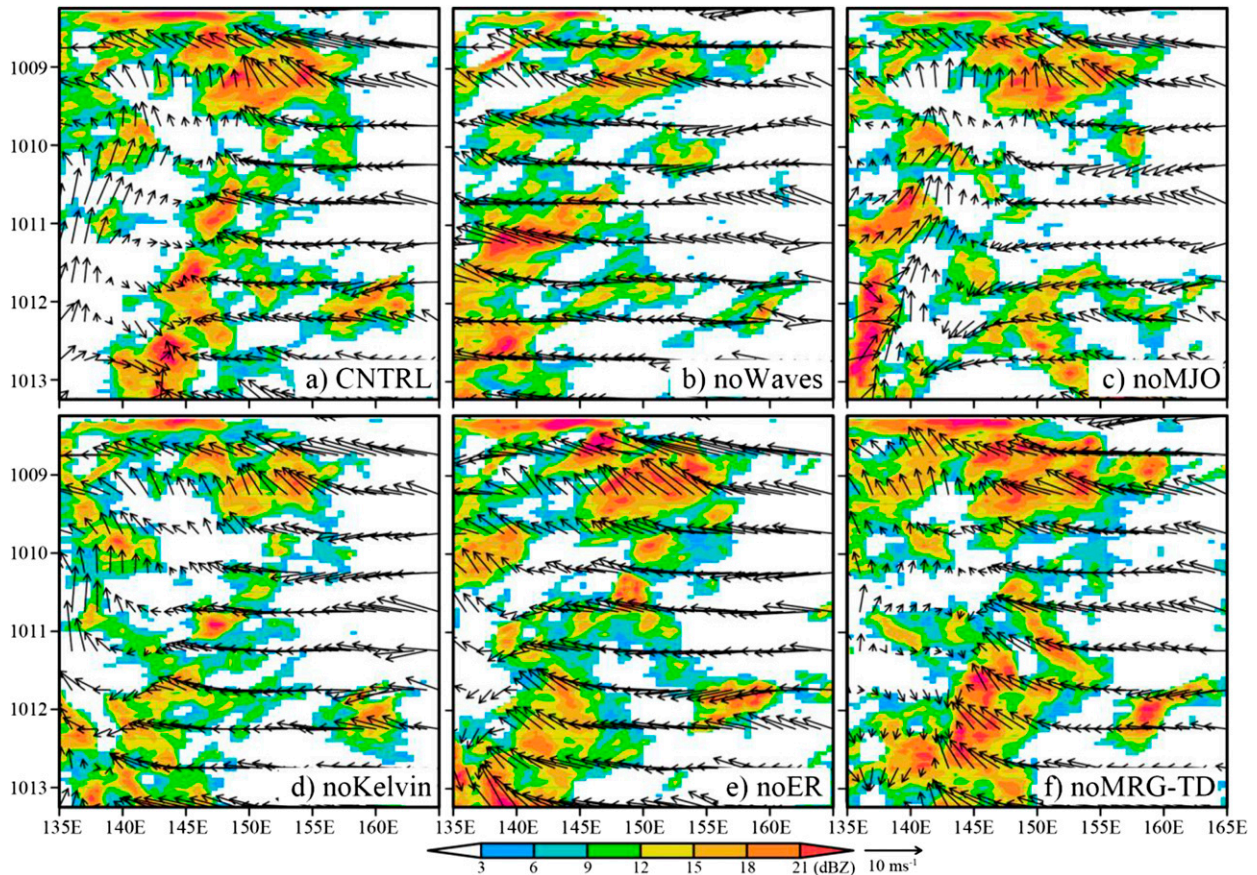


FIG. 11. Time–longitude section of model-derived column-maximum reflectivity averaged between 6° and 16°N (shading) and 850-hPa winds averaged between 9° and 13°N (vectors) in the period from 0600 UTC 8 Oct to 0600 UTC 13 Oct.

vorticity aggregation, development of low-level southwesterly, convection reignition, and rapid vorticity enhancement—all happened sequentially in noMJO. However, noMJO-derived convection as well as low-level winds and vorticity demonstrated remarkable differences from that in CNTRL in the western tropical Pacific. On the one hand, because of the reduced low-level convergence and cyclonic vorticity and specific humidity in the region embedding the PVAs owing to removal of the MJO from the initial fields (Figs. 10c,d), convection was slightly weaker in the northern tropical Pacific between 140° and 155°E before 1200 UTC 9 October in noMJO (Fig. 11c). The relatively weak convection together with the large-scale low-level divergence anomaly imposed by removing the MJO led to less effective aggregation of PVAs than that in CNTRL. From Fig. 12c, we can see that PVA B draws in the positive vorticity at the eastern tip of PVA C but fails to become a large PVA equivalent to that in CNTRL without merging with PVA A at 0600 UTC 10 October. On the other hand, along with the decay of convection near 145°E after around 0600 UTC 9 October (Fig. 11c),

the low-level flow in the near west of 145°E ceased to rotate clockwise with time but instead shifted back to be southeasterly most likely owing to adjustment of convection-yielded unbalance between the mass and momentum fields. Meanwhile, because of the evident low-level westerly anomaly induced by removing MJO to the west of 140°E (Fig. 10c),³ the zonal wind there was always about 2 m s^{-1} larger than that in CNTRL before 1200 UTC 9 October (Fig. 12c), which tended to enhance the convergence at about 140°E as the low-level winds shifted back to be southeasterly in the near west of 145°E (Fig. 11c). As a result, convection occurring near 140°E was stronger in noMJO than that in CNTRL after about 1800 UTC 9 October. Convection in turn strengthened the low-level westerly in its west

³ At 0600 UTC 8 Oct 2010, the main body of MJO's convective envelope was situated to the west of 130°E (Fig. 4d). Correspondingly, the MJO contributed to the enhancement of low-level easterly winds to the east of 130°E . Hence, the removal of the MJO tended to induce low-level westerly anomalies to the east of 130°E .

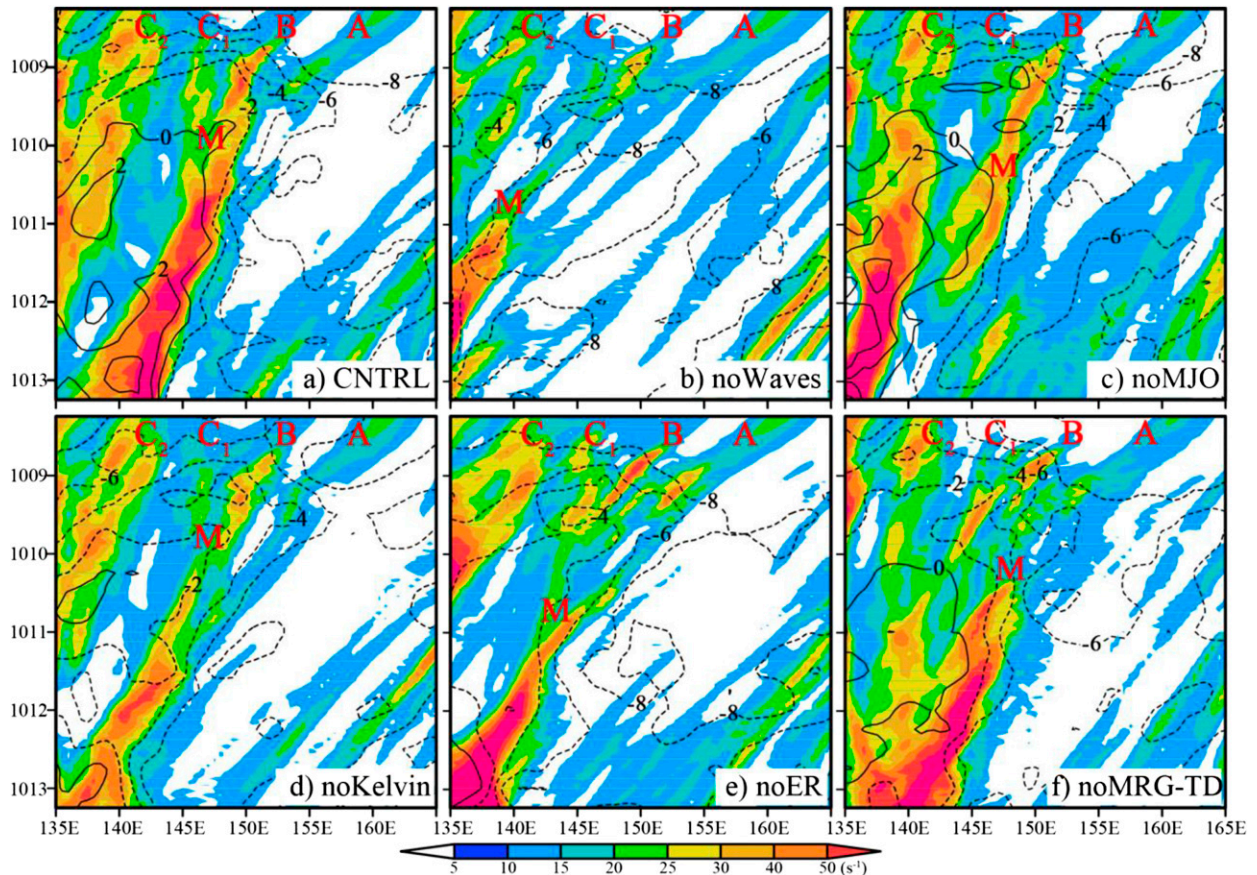


FIG. 12. Time-longitude section of model-derived 850-hPa vorticity averaged between 8° and 16°N (shading) and 850-hPa zonal wind speed averaged between 9° and 13°N (contours; m s^{-1}) in the period from 0600 UTC 8 Oct to 0600 UTC 13 Oct.

side, which was conducive to convection in the area near 140°E later. Accordingly, PVA C2 in that region was strengthened significantly and became stronger than PVA M located at 145°E after 1200 UTC 10 October. In the following several days, PVA C2 intensified gradually and developed into a TC in the far west of CNTRL-modeled Megi at 0000 UTC 13 October in noMJO. During this period, PVA M was partially wrapped into PVA C2 after about 0000 UTC 11 October (Fig. 12c).

3) EVOLUTION OF PVAS AND CONVECTION IN NOKELVIN

The noKelvin-simulated convection and vorticity in the PVAs evolved in a manner quite similar to that in CNTRL except for their relatively weaker intensity (Figs. 11d, 12d). From Figs. 10e and 10f, we can see that, because of the removal of Kelvin waves, the low-level convergence, low-to-midlevel moisture, and surface-based convective available potential energy (CAPE) decreased in the northern tropical Pacific between 140° and 155°E while the situation was reversed to the west of about

140°E . Consequently, noKelvin-simulated convection was considerably weaker than that in CNTRL in the region between 140° and 155°E while convection to the west of 140°E tended to be slightly stronger than that in CNTRL before 0600 UTC 10 October (Fig. 11d). Such a modification on convection caused the weakening of low-level easterly to be less evident to the west of 150°E before 0600 UTC 10 October and, thus, was less favorable for the increase of low-level convergence in the region embedding PVAs A, B, and the eastern part of C (i.e., C1) (Fig. 12d). As a result, the merger and intensification of the PVAs in noKelvin did not happen as efficiently as that in CNTRL. Although PVAs A, B, and C1 finally merged into a large PVA after around 1200 UTC 10 October, the vortex was too weak to develop into a TC at the genesis time of the observed Megi (Fig. 8d).

4) EVOLUTION OF PVAS AND CONVECTION IN NOER

In agreement with that inferred from Figs. 10g and 10h, noER-simulated convection and vorticity enhancement were much more notable in the northern tropical

Pacific between 140° and 155°E before 0000 UTC 10 October (Figs. 11e, 12e). Because of the low-level anticlockwise circulation anomaly induced by removing the ER wave in the western tropical Pacific (Fig. 10g), the west-northwestward movement of PVAs A, B, and eastern part of PVA C (i.e., C1) was faster in noER than that in CNTRL. At 0000 UTC 10 October, the PVA that resulted from the merger of PVAs A, B, and C1 in noER was about 400 km ahead of its counterpart in CNTRL and situated at around 145°E, where the low-level divergence and negative vorticity anomalies imposed by removing the ER wave were remarkable (Figs. 10g,h and Fig. 12e). Furthermore, the western part of PVA C (i.e., C2) moved to the west of 140°E and became located in the region with low-level convergence and positive CAPE anomalies induced by removing the ER wave after about 1200 UTC 9 October (Fig. 10g). Subsequently, convection and low-level vorticity enhancement took place in that region (Figs. 11e, 12e). The relatively strong convection to the west of 140°E was unfavorable for the development of low-level westerly flow to the west of PVA M and then the low-level convergence around the PVA. Therefore, PVA M did not intensify effectively after 1200 UTC 9 October in noER. At around 0000 UTC 11 October, PVA M merged with the PVA on its east side and intensified considerably. However, it was much weaker and thinner than that in CNTRL. In the following two days, the PVA intensified evidently but failed to develop into a TC at 0000 UTC 13 October (Fig. 8e).

5) EVOLUTION OF PVAS AND CONVECTION IN NOMRG-TD

Although the removal of MRG-TD-type waves weakened the vorticity of PVAs A and B and that in the eastern tip of C, it increased the low-level convergence and vorticity, low-to-midlevel moisture, and surface-based CAPE to the south of PVAs A and B and, thus, promoted the local enhancement of convection and vorticity (Figs. 10i,j). Hence, the latitude-averaged convection and low-level cyclonic vorticity in noMRG-TD were as evident as that in CNTRL in the northern tropical Pacific before 1200 UTC 9 October (Figs. 11f, 12f). However, owing to the low-level divergence anomalies associated with the removal of MRG-TD-type waves in the eastern part of the northwestern Pacific (Fig. 10j), the intensification and merger of PVAs A and B and new PVAs did not go well in noMRG-TD. The large PVA similar to PVA M in CNTRL did not form until 0900 UTC 10 October when the PVAs situated in the region of remarkably enhanced low-level convergence and cyclonic vorticity caused by removing the MRG-TD-type waves (Fig. 12f). After that, the convection and vorticity enhancement in PVA M as well as the low-level westerly flow to the

west of the PVA became notable as that in CNTRL. Moreover, because of the relatively weak convection near 140°E and its west over the period from 1200 UTC 9 October to 1200 UTC 10 October, PVA C2 did not intensify as effectively as that in CNTRL and was wrapped into PVA M gradually. At 0000 UTC 13 October, PVA M developed into a TC with intensity and location close to that in CNTRL (Fig. 8f).

c. Mesoscale processes in the formation of Megi in control and sensitivity experiments

This section focuses on the influence of tropical waves on the mesoscale processes in the inner-core area of model-derived precursors (area within a 2° radius of the vorticity center at 850 hPa) in the control and sensitivity experiments. Figures 13a and 13b exhibit the time–pressure diagrams of inner-core-averaged variables in CNTRL. Corresponding to the three-stage formation indicated by the evolution of convection and PVAs in the northwestern Pacific, the mesoscale processes in the inner core of CNTRL-simulated precursor could also be partitioned into three stages. Stage 1 (from 0600 UTC 8 October to 0600 UTC 9 October) was characterized by deep convection burst (Fig. 13a). As the unstable energy was consumed, the inner-core convection weakened and the precursor evolved into stage 2. Figures 13a and 13b show that, after about 0600 UTC 9 October, the downdrafts became dominant in the low levels while the updrafts mainly located in the middle and upper troposphere. Accordingly, divergence occurred in both the low and upper levels while the vorticity enhancement and convergence appeared in the middle troposphere. Such features meant that stratiform precipitation took place after the severe convection in the inner-core area of CNTRL-derived precursor (Mapes and Houze 1995). After about 0600 UTC 10 October, convection reinvigorated and the precursor evolved into stage 3. The persistent vigorous convection caused the lower troposphere to be dominated by convergence in the inner-core region of the precursor (Fig. 13b). Despite the obvious tendency of downward penetration of the midlevel positive vorticity exhibited at the beginning of stage 3, the vorticity budget based on the following equation⁴:

⁴ In Eq. (1), ζ is the relative vorticity and C is the moving velocity of the precursor determined by the displacement of the 850-hPa vorticity center. The terms on the right-hand side of Eq. (1) represent contributions to the change of ζ due to horizontal advection and convergence, vertical advection, and tilting effects. Since the solenoidal term and horizontal components of subgrid-scale terms generally yield small contribution to the net vorticity tendency, they have been ignored in Eq. (1) following Montgomery et al. (2006).

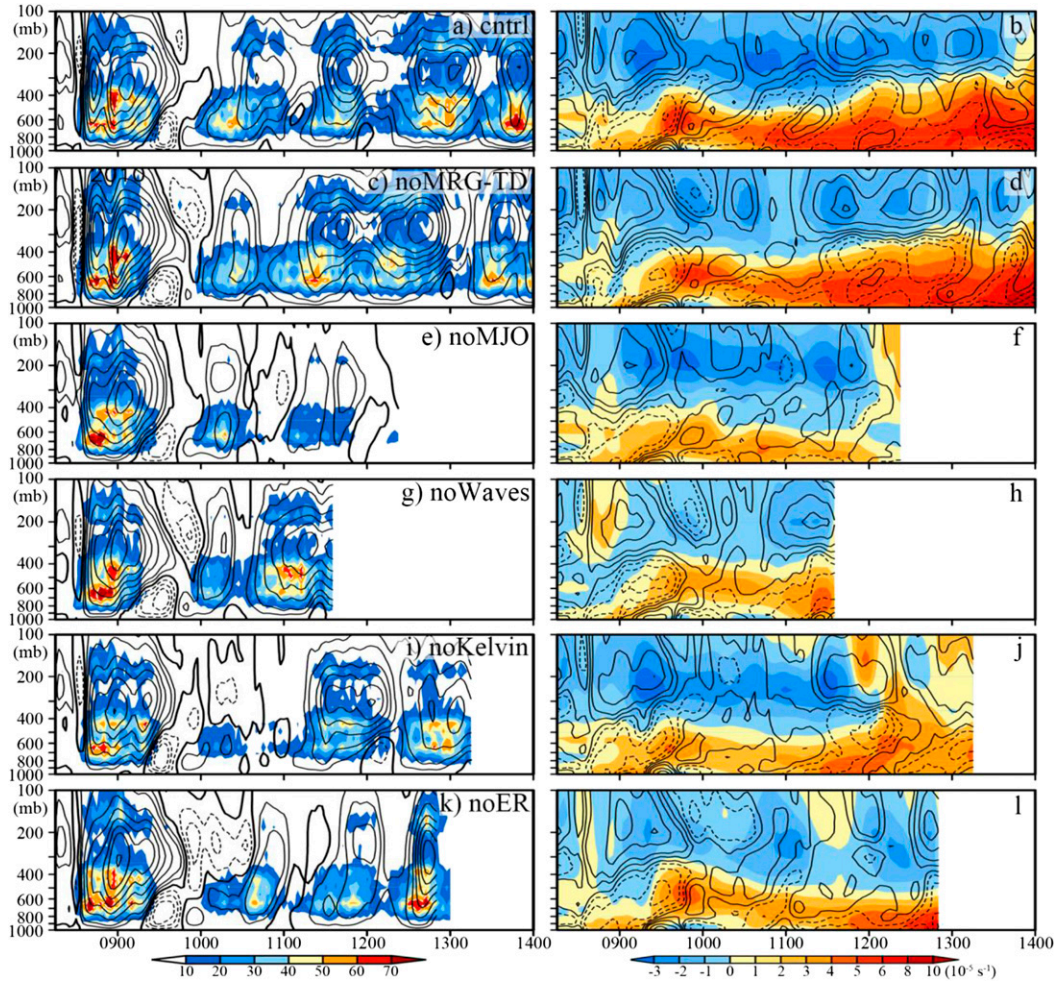


FIG. 13. (left) Time–height diagrams of model-derived mean frequency of convection top height (shading) and vertical velocity (contours) averaged over the inner-core area of Megi’s precursor. (right) As in (left), but for vorticity (shading) and horizontal divergence (contours). The values of contours are $-3, -2, -1, 0, 1, 2, 4, 6, 8, 10, 12, 15, 18, 21, 24, 27,$ and 30 cm s^{-1} in (left) and $0, \pm 0.5 \times 10^{-5}, \pm 1 \times 10^{-5}, \pm 2 \times 10^{-5}, \pm 3 \times 10^{-5}, \pm 4 \times 10^{-5},$ and $\pm 5 \times 10^{-5} \text{ s}^{-1}$ in (right). The negative contours are dashed.

$$\begin{aligned} \frac{\partial \zeta}{\partial t} = & -(\mathbf{V}_h - \mathbf{C}) \cdot \nabla_h (\zeta + f) - (\zeta + f) \nabla_h \cdot \mathbf{V}_h \\ & - w \frac{\partial \zeta}{\partial z} - \left(\frac{\partial w}{\partial x} \frac{\partial v}{\partial z} - \frac{\partial w}{\partial y} \frac{\partial u}{\partial z} \right), \end{aligned} \quad (1)$$

manifests that the increase of inner-core low-level vorticity was mainly caused by low-level convergence in stage 3 (Figs. 14a,b). Although the downward advection led to positive vorticity tendency in the inner-core region at $z = 1 \text{ km}$ after 0000 UTC 10 October as suggested by Bister and Emanuel (1997) (figure not shown), the tilting effect was so great that it nearly offset the positive vorticity tendency caused by vertical advection (Fig. 14b). As a result, the total vorticity tendency contributed from the vertical motion was too weak to cause significant increase of low-level vorticity in the inner

core of the precursor in stage 3. On the contrary, the stretching term linked with low-level convergence not only counteracted the negative role of horizontal advection term but also has surplus to strengthen the low-level inner-core vorticity noticeably (Fig. 14a). As the low-level vorticity increased, the positive vorticity demonstrated evident upward expansion (Fig. 13b). When the precursor developed into a TC at 0000 UTC 13 October, the positive vorticity had expanded to 200 hPa. Therefore, the early development of Megi was essentially a bottom–up process in CNTRL (Hendricks et al. 2004; Montgomery et al. 2006; Fang and Zhang 2010).

The three stages and bottom–up process also occurred in the inner core of noMRG–TD-simulated precursor (Figs. 13c,d and Figs. 14c,d). Although the inner-core convection was relatively weak at the beginning of stage

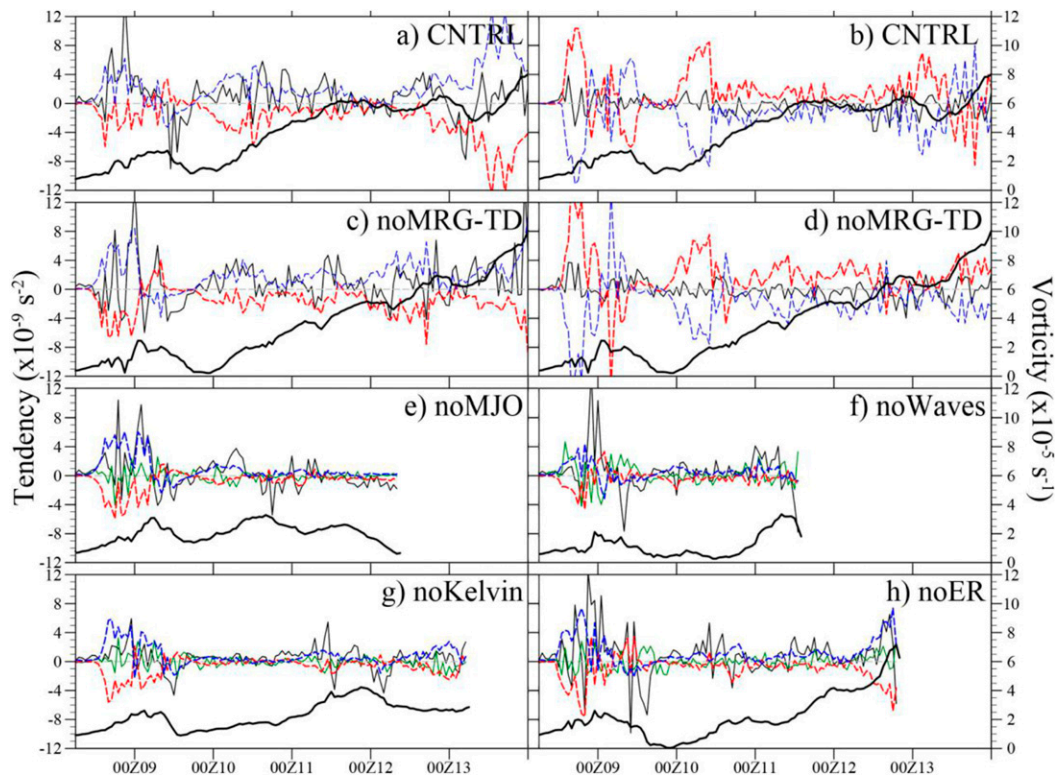


FIG. 14. (a) Time evolution of inner-core-averaged 1000-m vorticity (thick black) and vorticity tendency induced by horizontal advection (red), stretching effect (blue), and their summation (thin black) in CNTRL. (b) As in (a), but for the vorticity tendency induced by vertical advection (red), tilting effect (blue), and their summation (thin black). (c),(d) As in (a),(b), but for noMRG-TD. (e)–(h) As in (a), but for (e) noMJO, (f) noWaves, (g) noKelvin, and (h) noER. The green curves denote the vorticity tendency induced by the vertical advection and tilting effect in (e)–(h). The summation of horizontal advection and stretching terms and vertical advection and tilting terms was multiplied by 4 for clarity.

3, it became vigorous after 0000 UTC 11 October, when the precursor was situated in the region with distinctively enhanced low-level convergence and low-to-midlevel moisture caused by removal of the MRG-TD-type waves, which led to the formation of a TC 2 days later.

Similar to that in CNTRL and noMRG-TD, the inner core of model-simulated precursors also experienced deep convective burst, stratiform process, and convection reinvigoration in the other four sensitivity experiments (Figs. 13e–l). However, the inner-core convection was weaker than that in CNTRL and noMRG-TD in stage 3 in these experiments on the whole. In noMJO (Fig. 13e), the mean vertical velocity remained very small and there was only sporadic deep convection that reached 200 hPa in the inner-core area after 0600 UTC 10 October. Correspondingly, the inner-core convergence and induced vorticity tendency was very weak in the lower troposphere in stage 3 (Figs. 13f, 14e). Hence, the precursor failed to develop into a TC before it was wrapped into the PVA to the west in noMJO. In noWaves

and noKelvin, only shallow convection or congestus was active in the inner-core area of the precursor at the beginning of stage 3 (Figs. 13g,h and 13i,j). Although deep convection burst later, it was not strong enough to induce a remarkable stretching effect to spin up the low-level vortex efficiently before it moved out the model domain (Figs. 13g,h and 13i,j and Figs. 14f,g). From Fig. 13k, we can see that deep convection burst after 1200 UTC 12 October in the inner-core area in noER, which resulted in a distinct stretching effect and increase of inner-core vorticity at 1000 hPa (Figs. 13l, 14h). However, because of the relatively weak convection in the period from 0000 UTC 10 October to 1200 UTC 12 October (Fig. 13k), the low-level cyclonic vortex was much shallower in noER than that in CNTRL (Fig. 13l) and failed to develop into a TC at the time and location close to that of CNTRL-simulated Megi (Fig. 8e). From the above description, we can see that the deep convection reinvigorated in stage 3 played a critical role in the spinup of a TC. Without the MJO and tropical waves, the inner-core deep convection

was considerably weaker than that in CNTRL, and thus the precursor failed to become a TC in noMJO, noKelvin, noER, or noWaves at the genesis time of CNTRL-simulated Megi.

5. Concluding remarks

Through observational analysis and convection-permitting WRF simulations, the roles of tropical waves including the MJO in the formation of Super typhoon Megi are examined in this study. The formation of Megi is found to involve three westward-moving low-level disturbances with positive vorticity (i.e., PVAs A, B, and C), initially aligned from the east to west in the western tropical Pacific. Based on the sequence of convective processes and evolution of the PVAs obtained from the GMS/MTSAT and GFS data, three stages of Megi's formation were identified: 1) massive deep convection, vorticity aggregation, and formation of Megi's embryo; 2) convection decaying and vortex rearrangement; and 3) reinvigoration of deep convection, vortex intensification, and formation of a TD. The key processes in these three stages were facilitated by the equatorial waves considerably.

The MJO preconditioned the large-scale background environment and caused remarkable low-level convergence and positive vorticity and low-to-midlevel moisture anomalies favorable for the formation of Megi in the western tropical Pacific. As the westernmost PVA (i.e., C) moved westward preconditioned by the MJO, passing of two consecutive Kelvin waves steered the eastward extension of the low-level westerly and boosted deep moist convection in the northwestern Pacific, which promoted the intensification of PVA C and formation of PVA B in its east side as well as slowed down their westward propagation. Subsequently, PVA B was caught by PVA A initially related to an MRG–TD-type wave from the central Pacific and then draw in the vorticity in the eastern tip of PVA C to become the embryo of Megi at the end of stage 1. Via conditioning the low-level convergence and vorticity in the region embedding the PVAs directly, the ER wave not only facilitated the above-mentioned processes in stage 1 but also contributed to the intensification of Megi's precursor in stages 2 and 3. Moreover, the ER- and MRG–TD-type waves worked jointly to promote the development of low-level southwesterly to the southwest of the precursor, which contributed to the precursor's intensification via transporting positive vorticity in its front edge to the precursor in stages 2 and 3.

The tropical waves affected the formation of Megi not only directly via preconditioning the environment of the precursor but also indirectly through modifying the perturbations in the neighborhood. Without the MJO,

the low-level convergence, cyclonic vorticity, and specific humidity in most of the region embedding the PVAs were relatively weak, which were less favorable for convection and aggregation of vorticity in the PVAs. Therefore, PVA M resulting from the PVAs was relatively weaker and smaller in noMJO. Meanwhile, the removal of the MJO caused the PVA to the west of PVA M to develop too fast and finally draw in PVA M to become a TC too far west instead of the observed Megi. In the case that the Kelvin waves were removed, relatively weaker convection in the region around PVA A, B, and the eastern part of PVA C and slightly enhanced convection in the western part of PVA C caused the low-level easterly flow to be stronger than that in CNTRL in the northern tropical Pacific west of 150°E. Under the effect of the strong easterly, PVAs A, B, and the eastern part of C (PVA M later) intensified and aggregated slowly while it moved westward faster. Despite the fact that PVAs A, B, and the eastern part of C were strengthened considerably in stage 1 in noER, relatively stronger convection appearing to the west of the PVAs was also less favorable for the weakening of low-level easterly flow in its east and then the intensification of PVA M just as that in noKelvin. Hence, PVA M failed to develop into a TC at 0000 UTC 13 October in both noKelvin and noER.

With regard to the three-stage formation of Megi, the combined effect of the MJO, Kelvin, and ER waves was very important to the reinvigoration of deep convection in the inner-core region of the precursor in stage 3 and, thus, to the formation of Megi. As a contrast, the MRG–TD-type waves seemed to play a less critical role in the formation of Megi because noMRG–TD also simulated a TC with genesis time and location close to that in CNTRL. However, the remarkable differences of the PVAs' evolution from that in CNTRL in the northwestern Pacific show that it is the MRG–TD-type wave that worked jointly with the MJO and other waves to make the PVAs evolve and organize into TC Megi in a specific way. In this specific way, MRG–TD-type wave could be very important via providing low-level convergence, cyclonic vorticity, moisture, and southwesterly anomalies as shown in Fig. 3d and Figs. 6d–e.

Acknowledgments. The authors are grateful for the constructive comments provided by Da-Lin Zhang, Carl Schreck, and two anonymous reviewers of the manuscript. This work was supported in part by Nature Science Foundation of China Grants 41475046, 4141101079, and 41130964; State Key Basic Program of China 2012CB417201; U.S. Office of Naval Research Grant N000140910526; and National Science Foundation Grant AGS 1305798. Computing was performed at the Texas Advanced Computing Center.

REFERENCES

- Aiyyer, A. R., and J. Molinari, 2003: Evolution of mixed Rossby-gravity waves in idealized MJO environments. *J. Atmos. Sci.*, **60**, 2837–2855, doi:10.1175/1520-0469(2003)060<2837:EOMRWI>2.0.CO;2.
- Bessafi, M., and M. C. Wheeler, 2006: Modulation of south Indian Ocean tropical cyclones by the Madden-Julian oscillation and convectively coupled equatorial waves. *Mon. Wea. Rev.*, **134**, 638–656, doi:10.1175/MWR3087.1.
- Bister, M., and K. A. Emanuel, 1997: The genesis of Hurricane Guillermo: TEXMEX analyses and a modeling study. *Mon. Wea. Rev.*, **125**, 2662–2682, doi:10.1175/1520-0493(1997)125<2662:TGOHGT>2.0.CO;2.
- Chen, G., 2012: A comparison of the transition of equatorial waves between two types of ENSO events in a multilevel model. *J. Atmos. Sci.*, **69**, 2364–2378, doi:10.1175/JAS-D-11-0292.1.
- , and R. Huang, 2009: Interannual variation of the mixed Rossby-gravity waves and their impact on tropical cyclogenesis in the western North Pacific. *J. Climate*, **22**, 535–549, doi:10.1175/2008JCLI2221.1.
- , and C. Chou, 2014: Joint contribution of multiple equatorial waves to tropical cyclogenesis over the western North Pacific. *Mon. Wea. Rev.*, **142**, 79–93, doi:10.1175/MWR-D-13-00207.1.
- Ching, L., C.-H. Sui, and M.-J. Yang, 2010: An analysis of the multiscale nature of tropical cyclone activities in June 2004: Climate background. *J. Geophys. Res.*, **115**, D24108, doi:10.1029/2010JD013803.
- Dickinson, M., and J. Molinari, 2002: Mixed Rossby-gravity waves and western Pacific tropical cyclogenesis. Part I: Synoptic evolution. *J. Atmos. Sci.*, **59**, 2183–2196, doi:10.1175/1520-0469(2002)059<2183:MRGWAW>2.0.CO;2.
- Dudhia, J., 1989: Numerical study of convection observed during the Winter Monsoon Experiment using a mesoscale two-dimensional model. *J. Atmos. Sci.*, **46**, 3077–3107, doi:10.1175/1520-0469(1989)046<3077:NSOCOD>2.0.CO;2.
- Dunkerton, T. J., M. T. Montgomery, and Z. Wang, 2009: Tropical cyclogenesis in a tropical wave critical layer: Easterly waves. *Atmos. Chem. Phys.*, **9**, 5587–5646, doi:10.5194/acp-9-5587-2009.
- Fang, J., and F. Zhang, 2010: Initial development and genesis of Hurricane Dolly (2008). *J. Atmos. Sci.*, **67**, 655–672, doi:10.1175/2009JAS3115.1.
- Frank, W. M., and P. E. Roundy, 2006: The role of tropical waves in tropical cyclogenesis. *Mon. Wea. Rev.*, **134**, 2397–2417, doi:10.1175/MWR3204.1.
- Gray, W. M., 1968: Global view of the origin of tropical disturbances and storms. *Mon. Wea. Rev.*, **96**, 669–700, doi:10.1175/1520-0493(1968)096<0669:GVOTOO>2.0.CO;2.
- Hendricks, E. A., M. T. Montgomery, and C. A. Davis, 2004: The role of “vortical” hot towers in the formation of Tropical Cyclone Diana (1984). *J. Atmos. Sci.*, **61**, 1209–1232, doi:10.1175/1520-0469(2004)061<1209:TROVHT>2.0.CO;2.
- Hogsett, W., and D.-L. Zhang, 2010: Genesis of Typhoon Chancho (2006) from a westerly wind burst associated with the MJO. Part I: Evolution of a vertically tilted precursor vortex. *J. Atmos. Sci.*, **67**, 3774–3792, doi:10.1175/2010JAS3446.1.
- Holland, G. J., 1995: Scale interaction in the western Pacific monsoon. *Meteor. Atmos. Phys.*, **56**, 57–79, doi:10.1007/BF01022521.
- Hong, S.-Y., J. Dudhia, and S.-H. Chen, 2004: A revised approach to ice microphysical processes for the parameterization of clouds and precipitation. *Mon. Wea. Rev.*, **132**, 103–120, doi:10.1175/1520-0493(2004)132<0103:ARATIM>2.0.CO;2.
- Huffman, G. J., and Coauthors, 2007: The TRMM Multisatellite Precipitation Analysis (TMPA): Quasi-global, multiyear, combined-sensor precipitation estimates at fine scales. *J. Hydrometeorol.*, **8**, 38–55, doi:10.1175/JHM560.1.
- Janicot, S., F. Mounier, N. M. J. Hall, S. Leroux, B. Sultan, and G. N. Kiladis, 2009: Dynamics of the West African monsoon. Part IV: Analysis of 25–90-day variability of convection and the role of the Indian monsoon. *J. Climate*, **22**, 1541–1565, doi:10.1175/2008JCLI2314.1.
- Kieu, C. Q., N. M. Truong, H. T. Mai, and N.-D. Thanh, 2012: Sensitivity of the track and intensity forecasts of Typhoon Megi (2010) to satellite-derived atmospheric motion vectors with the ensemble Kalman filter. *J. Atmos. Sci.*, **29**, 1794–1810, doi:10.1175/JTECH-D-12-00020.1.
- Kiladis, G. N., M. C. Wheeler, P. T. Haertel, K. H. Straub, and P. E. Roundy, 2009: Convectively coupled equatorial waves. *Rev. Geophys.*, **47**, RG2003, doi:10.1029/2008RG000266.
- Ko, D. S., S.-Y. Chao, C.-C. Wu, and I.-I. Lin, 2014: Impacts of Typhoon Megi (2010) on the South China Sea. *J. Geophys. Res. Oceans*, **119**, 4474–4489, doi:10.1002/2013JC009785.
- Liebmann, B., and H. H. Hendon, 1990: Synoptic-scale disturbances near the equator. *J. Atmos. Sci.*, **47**, 1463–1479, doi:10.1175/1520-0469(1990)047<1463:SSDNTE>2.0.CO;2.
- , —, and J. D. Glick, 1994: The relationship between tropical cyclones of the western Pacific and Indian Oceans and the Madden-Julian oscillation. *J. Meteor. Soc. Japan*, **72**, 401–411.
- Maloney, E. D., and D. L. Hartmann, 1998: Frictional moisture convergence in a composite life cycle of the Madden-Julian oscillation. *J. Climate*, **11**, 2387–2403, doi:10.1175/1520-0442(1998)011<2387:FMCIAC>2.0.CO;2.
- , and —, 2000a: Modulation of eastern North Pacific hurricanes by the Madden-Julian oscillation. *J. Climate*, **13**, 1451–1460, doi:10.1175/1520-0442(2000)013<1451:MOENPH>2.0.CO;2.
- , and —, 2000b: Modulation of hurricane activity in the Gulf of Mexico by the Madden-Julian oscillation. *Science*, **287**, 2002–2004, doi:10.1126/science.287.5460.2002.
- , and —, 2001: The Madden-Julian oscillation, barotropic dynamics, and North Pacific tropical cyclone formation. Part I: Observations. *J. Atmos. Sci.*, **58**, 2545–2558, doi:10.1175/1520-0469(2001)058<2545:TMJOBOD>2.0.CO;2.
- Mapes, B. E., and R. A. Houze Jr., 1995: Diabatic divergence profiles in western Pacific mesoscale convective systems. *J. Atmos. Sci.*, **52**, 1807–1828, doi:10.1175/1520-0469(1995)052<1807:DDPIWP>2.0.CO;2.
- Masunaga, H., 2007: Seasonality and regionality of the Madden-Julian oscillation, Kelvin wave, and equatorial Rossby wave. *J. Atmos. Sci.*, **64**, 4400–4416, doi:10.1175/2007JAS2179.1.
- Matthews, A. J., 2004: Intraseasonal variability over tropical Africa during northern summer. *J. Climate*, **17**, 2427–2440, doi:10.1175/1520-0442(2004)017<2427:IVOTAD>2.0.CO;2.
- Mlawer, E. J., S. J. Taubman, P. D. Brown, M. J. Iacono, and S. A. Clough, 1997: Radiative transfer for inhomogeneous atmospheres: RRTM, a validated correlated-*k* model for the longwave. *J. Geophys. Res.*, **102**, 16 663–16 682, doi:10.1029/97JD00237.
- Molinari, J., D. Knight, M. Dickinson, D. Vollaro, and S. Skubis, 1997: Potential vorticity, easterly waves, and eastern Pacific tropical cyclogenesis. *Mon. Wea. Rev.*, **125**, 2699–2708, doi:10.1175/1520-0493(1997)125<2699:PVEWAE>2.0.CO;2.
- , K. Lombardo, and D. Vollaro, 2007: Tropical cyclogenesis within an equatorial Rossby wave packet. *J. Atmos. Sci.*, **64**, 1301–1317, doi:10.1175/JAS3902.1.

- Montgomery, M. T., M. E. Nicholls, T. A. Cram, and A. B. Saunders, 2006: A vortical hot tower route to tropical cyclogenesis. *J. Atmos. Sci.*, **63**, 355–386, doi:10.1175/JAS3604.1.
- Noh, Y., W. G. Cheon, S. Y. Hong, and S. Raasch, 2003: Improvement of the *K*-profile model for the planetary boundary layer based on large eddy simulation data. *Bound.-Layer Meteor.*, **107**, 401–427, doi:10.1023/A:1022146015946.
- Qian, C., F. Zhang, B. W. Green, J. Zhang, and X. Zhou, 2013: Probabilistic evaluation of the dynamics and prediction of Supertyphoon Megi (2010). *Wea. Forecasting*, **28**, 1562–1577, doi:10.1175/WAF-D-12-00121.1.
- Roundy, P. E., 2008: Analysis of convectively coupled Kelvin waves in the Indian Ocean MJO. *J. Atmos. Sci.*, **65**, 1342–1359, doi:10.1175/2007JAS2345.1.
- Schreck, C. J., 2015: Kelvin waves and tropical cyclogenesis: A global survey. *Mon. Wea. Rev.*, **143**, 3996–4011, doi:10.1175/MWR-D-15-0111.1.
- , and J. Molinari, 2009: A case study of an outbreak of twin tropical cyclones. *Mon. Wea. Rev.*, **137**, 863–875, doi:10.1175/2008MWR2541.1.
- , and —, 2011: Tropical cyclogenesis associated with Kelvin waves and the Madden-Julian oscillation. *Mon. Wea. Rev.*, **139**, 2723–2734, doi:10.1175/MWR-D-10-05060.1.
- , —, and K. I. Mohr, 2011: Attributing tropical cyclogenesis to equatorial waves in the western North Pacific. *J. Atmos. Sci.*, **68**, 195–209, doi:10.1175/2010JAS3396.1.
- , —, and A. Aiyyer, 2012: A global view of equatorial waves and tropical cyclogenesis. *Mon. Wea. Rev.*, **140**, 774–788, doi:10.1175/MWR-D-11-00110.1.
- Shen, B.-W., W.-K. Tao, Y.-L. Lin, and A. Laing, 2012: Genesis of twin tropical cyclones as revealed by a global mesoscale model: The role of mixed Rossby gravity waves. *J. Geophys. Res.*, **117**, D13114, doi:10.1029/2012JD017450.
- Shi, W., J. Fei, X. Huang, X. Cheng, J. Ding, and Y. He, 2014: A numerical study on the combined effect of midlatitude and low-latitude systems on the abrupt track deflection of Typhoon Megi (2010). *Mon. Wea. Rev.*, **142**, 2483–2501, doi:10.1175/MWR-D-13-00283.1.
- Shu, S., and F. Zhang, 2015: Influence of equatorial waves on the genesis of Super Typhoon Haiyan (2013). *J. Atmos. Sci.*, **72**, 4591–4613, doi:10.1175/JAS-D-15-0016.1.
- Skamarock, W. C., and J. B. Klemp, 2008: A time-split nonhydrostatic atmospheric model for weather research and forecasting applications. *J. Comput. Phys.*, **227**, 3465–3485, doi:10.1016/j.jcp.2007.01.037.
- Sobel, A. H., and E. D. Maloney, 2000: Effect of ENSO and the MJO on western North Pacific tropical cyclones. *Geophys. Res. Lett.*, **27**, 1739–1742, doi:10.1029/1999GL011043.
- Straub, K. H., and G. N. Kiladis, 2003: Interactions between the boreal summer intraseasonal oscillation and higher-frequency tropical wave activity. *Mon. Wea. Rev.*, **131**, 945–960, doi:10.1175/1520-0493(2003)131<0945:IBTBSI>2.0.CO;2.
- Takayabu, Y. N., and T. Nitta, 1993: 3–5 day-period disturbances coupled with convection over the tropical Pacific Ocean. *J. Meteor. Soc. Japan*, **71**, 221–245.
- Ventrice, M. J., C. D. Thorncroft, and M. A. Janiga, 2012a: Atlantic tropical cyclogenesis: A three-way interaction between an African easterly wave, diurnally varying convection, and a convectively coupled atmospheric Kelvin wave. *Mon. Wea. Rev.*, **140**, 1108–1124, doi:10.1175/MWR-D-11-00122.1.
- , —, and C. J. Schreck, 2012b: Impacts of convectively coupled Kelvin waves on environmental conditions for Atlantic tropical cyclogenesis. *Mon. Wea. Rev.*, **140**, 2198–2214, doi:10.1175/MWR-D-11-00305.1.
- Wang, H., and Y. Wang, 2014: A numerical study of Typhoon Megi (2010). Part I: Rapid intensification. *Mon. Wea. Rev.*, **142**, 29–48, doi:10.1175/MWR-D-13-00070.1.
- Wang, Y., and H. Wang, 2013: The inner-core size increase of Typhoon Megi (2010) during its rapid intensification phase. *Trop. Cyclone Res. Rev.*, **2**, 65–80, doi:10.6057/2013TCRR02.01.
- Wang, Z., 2014: Characteristics of convective processes and vertical vorticity from the tropical wave to tropical cyclone stage in a high-resolution numerical model simulation of Tropical Cyclone Fay (2008). *J. Atmos. Sci.*, **71**, 896–915, doi:10.1175/JAS-D-13-0256.1.
- Webster, P. J., and H.-R. Chang, 1988: Equatorial energy accumulation and emanation regions: Impacts of a zonally varying basic state. *J. Atmos. Sci.*, **45**, 803–829, doi:10.1175/1520-0469(1988)045<0803:EEAAER>2.0.CO;2.
- Wheeler, M., and G. N. Kiladis, 1999: Convectively coupled equatorial waves: Analysis of clouds and temperature in the wavenumber–frequency domain. *J. Atmos. Sci.*, **56**, 374–399, doi:10.1175/1520-0469(1999)056<0374:CCEWAO>2.0.CO;2.
- Xu, Y., T. Li, and M. Peng, 2013: Tropical cyclogenesis in the western North Pacific as revealed by the 2008–09 YOTC data. *Wea. Forecasting*, **28**, 1038–1056, doi:10.1175/WAF-D-12-00104.1.
- Zhang, C., 2005: The Madden-Julian oscillation. *Rev. Geophys.*, **43**, RG2003, doi:10.1029/2004RG000158.